THE JOURNAL OF PHYSICAL CHEMISTRY B

Article

pubs.acs.org/JPCB

Influence of Protein Self-Association on Complex Coacervation with Polysaccharide: A Monte Carlo Study

Yunqi Li and Qingrong Huang*

Department of Food Science, Rutgers University, 65 Dudley Road, New Brunswick, New Jersey 08901, United States

Supporting Information

ABSTRACT: Coarse-grained Monte Carlo simulations have been applied to study complex coacervation of pectin with bovine serum albumin (BSA) and two isomers of beta-lactoglobulin (BLGA and BLGB). The influence from the specific distribution of charge and hydrophobic patches in protein surfaces on the self-association of proteins and their complex coacervation were investigated. A simple and direct method to quantify the contribution of hydrophobic interaction on protein complex formation was introduced. Highly accordant pH dependence of charges in proteins and phase boundaries for the complex coacervation was observed. Comparing to BSA, beta-lactoglobulin had a higher probability and a broader pH window to form complex coacervate. The major cause is the higher self-association proneness of beta-lactoglobulin, as evidenced by the more negative second virial coefficients. The double-point mutations of G64D/V118A from BLGB to BLGA caused the latter one to have a stronger self-association proneness. It was revealed that the larger negative charge patch in BLGA synergistically enhanced the attraction of the strongest binding site, a positive charge patch, when pH was close to or above the isoelectric point of the protein. These findings suggest that the coarse grained simulation is competent to explore the delicate influences from different proteins in protein−polysaccharide complex coacervates.

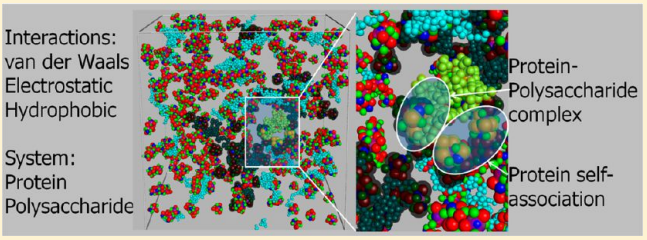

INTRODUCTION

Bovine serum albumin (BSA) and beta-lactoglobulin (BLG) are two commonly used model proteins in the development of pharmaceutical, cosmetic, and food formulations. Their capability to form complexes with various polyelectrolytes, especially with potent chargeable polysaccharides, has attracted broad interests for potential applications in encapsulation,[1−3] control-release delivery,[4,5] protein fraction,[6] and purification.[7] It is generally believed that electrostatic interactions dominate the association and the phase behavior in the protein−polysaccharide complex. Both extrinsic physicochemical conditions (e.g., pH and ionic concentration) and intrinsic features (e.g., distribution of charges, size, topological surface of proteins, stiffness of polysaccharide chains, etc.) can significantly influence the formation, the structure, and the property of the complex. Among all these factors, the influence of the self-association proneness of proteins is still far from clear.

Comparing BSA with the two isomers of BLG (BLGA and BLGB), the most significant difference may be their specific distributions of charged and hydrophobic groups in the protein surface, besides their differences in molecular weight, size, and contour shape. Although BLGA and BLGB only have two residue variances in their sequences, it may arouse remarkable differences from multiple aspects. In aqueous solutions, scientists found that the heterogeneity in milk proteins was made up of metastable dimers or oligomers that majorly contributed to the greater self-association proneness of BLGA than that of BLGB.[8−10] Later on, these oligomers were verified as transient clusters of proteins in high salt solutions.[11] Furthermore, in low ionic strength solutions, the self-association of BLG was found to be driven by electrostatic interaction coupled with the specific charge distribution of protein dimers.[12] On the contrary, BSA has very weak self-association proneness and a reversible fast dimerization equilibrium.[13] The underlying reason for the self-association proneness of proteins is still in the cutting-edge research, but other works focusing on their applications in delivery systems and their complexation capability with polysaccharide provided more evidence. For example, in the delivery of retinol, it has been found that BLGA has a better performance than either BLGB and BSA.[14] On the basis of quartz crystal microbalance with dissipation monitoring (QCMD) measurements, Noel et al. found that BSA and BLG show very different profiles and pH dependences when interacting with pectin in layer-by-layer deposition.[15] Recently, Chen et al. observed that the tiny difference between BLGA and BLGB had distinctive binding affinities to positive charged gold nanoparticles.[16] They interpreted that the difference was derived from a large negative charge patch in BLGA, which promoted the binding of protein to the nanoparticles. Xu et al. also found that BLG had a stronger affinity than BSA, and BLGA also had a stronger binding affinity than BLGB to interact with a polycation,

Received: September 14, 2012
Revised: January 30, 2013
Published: February 17, 2013

   dx.doi.org/10.1021/jp309135m | J. Phys. Chem. B 2013, 117, 2615−2624

Table 1. Parameters in the Coarse Grained Model-Based Protein Crystal Structures[a]

protein	PDB	length	size (nm)	positive	negative	hydrophobic	pI	pIa	self-association proneness
BSA	1e7i	585	2.84 (3.0)	100 (70)	117 (92)	246 (86)	4.66	5.87	weak
BLGB	1beb	162	1.48 (1.5)	21 (17)	31 (22)	78 (21)	5.14	5.19	intermediate
BLGA	3blg	162	1.48 (1.5)	21 (17)	32 (23)	77 (20)	4.96	5.03	strong

[a]Positive, negative, and hydrophobic provide the number of residues in proteins and those in the solvent accessible region (in parentheses). pI and pIa are the isoelectric point of proteins in consideration of all titratable residues and all chargeable residues, respectively. The relative self-association proneness is a consensus from multiple literature reports as described in the introduction section.

poly(diallyldimethylammonium chloride) (PDADMAC), and form complex coacervate.[7] They concluded that the difference comes from the anisotropic distribution of surface charges in these proteins. The majority of these works considered that the electrostatic interaction exclusively dominated the binding behaviors of different proteins. However, Kosters et al. used a set of peptide fragments from BLG to study their binding affinity with whole BLG and found that several fragments had a high binding affinity contributed to the self-association of proteins. They confirmed that the binding affinity is determined by the total hydrophobicity and the total charge of the peptides.[17,18] Moreover, Sperber and co-workers utilized fluorescence anisotropy and isothermal titration calorimetry (ITC) to investigate the effect of ionic strength on the cooperativities and isotherms during the binding of BLG with various types of pectin.[19,20] They found that small differences in either the chemical structure of pectin or the arrangement of waters associated hydrophobic interaction played an important role in the binding between protein and polysaccharide. In order to clarify the determinant contributions of protein self-association to the complexation with polysaccharides, applying Monte Carlo simulation in a comparative study of BSA and the two isomers of BLG may provide abundant information to help understand the complex behavior in such systems.

To simulate the binding and complexation behavior in protein and polysaccharide mixtures, where tons of atoms with highly asymmetric sizes are encountered, coarse graining is indispensable for constructing practicable protocols. Polysaccharide chains can be regarded as homogeneous polymers with evenly distributed partial charges along the chain. While the coarse grained model for proteins is much more complicated, a number of exhaustive reviews are available.[21−23]

In the situation where nonselective interactions, such as electrostatic interaction, van der Waals interaction, hydrophobic interaction etc., dominate the binding and the association of molecules, a high degree of coarse graining will allow simulation at large temporal and spatial scales. The simplest coarse grained protein model maybe the hard-sphere model,[24−27] which provided the overall steric repulsion and electrostatic interaction of an entire protein. Then the patchy colloid model[28] can present the anisotropic interaction and the specific shape of proteins. Further utilizing protein crystal structures deposited in protein data bank (PDB),[29−33] named as the exact model, can provide the detailed contour and surface features for a given protein. On the basis of the exact model, interactions and binding sites in the complex can be identified at residue level. Recently, we have developed Monte Carlo simulation models using either the patchy colloid model[34] or the exact model with a soft sphere associated with specific surface charge distribution.[35] Both simulations delivered consistent phase boundaries for the complex coacervation of BSA with a polycation or a polyanion, in comparison with turbidimetric titration experiments of the corresponding systems. Though these coarse grained models for proteins and the related simulation works have largely improved our understanding of complexation in protein and polysaccharide mixtures, further development to reveal more details is still needed. For example, how the hydrophobic interaction contributed to complexation has never been clearly stated. It has been reported that binding sites are highly overlapped with charge patches in proteins,[36] but the surface hydrophobic patch may also play an important role when proteins are binding to other molecules.[37,38]

In this work, Monte Carlo simulation is used to study the complex and complex coacervation in BSA, BLGA, BLGB, and pectin mixtures. Coarse grained models based on the characteristic distributions of surface charge and hydrophobic patches in proteins were setup first. Simulations guided by nonselective electrostatic, hydrophobic, and van der Waals interactions were subsequently carried out. Phase boundaries during complex coacervation were then determined by applying percolation concepts. Intermolecular interactions represented by second virial coefficients were analyzed. At molecular level, conformation of pectin chains and its dependence on the number of bound proteins and pH were studied. Finally, the strongest binding sites in proteins contributed to complexation and protein self-association were identified at the whole pH range.

SIMULATION METHODS

Coarse Grained Model. Similar to our previous work,[35] the coarse grained models for the three proteins BSA, BLGA, and BLGB were built based on their crystal structures from PDB. Key information is summarized in Table 1. Full length of protein structures were used as the referent structure, and the incomplete coordinates in the structures were added using REMO[39] according to their sequences presented in the head of PDB entry. Then exposed/buried residues in the full atomic structure were assigned using a threshold of 25% of the solvent accessible area calculated by DSSP.[40] Since surface residues should be accessible by other molecules, all titratable[41] and surface hydrophobic residues were limited to those exposed residues. The size is the gyration radius calculated from all atoms except hydrogen atoms based on the crystal structure from PDB and the van der Waals radius for the entire protein (in parentheses) was used in the coarse grained model. The pH dependence of the charges brought by each protein were then calculated and presented in Figure S1 (in Supporting Information), in consideration of all chargeable and titratable residues. The partial charge brought by each residue was calculated according to the basic−acidic equilibrium referring to the pK_a of the chemical groups, which can be protonated or disassociated to bring positive or negative charges. The pK_a values of ionizable groups were adopted from a recent report by Pace et al.[42] The isoelectric point (pI) calculated from titratable residues, rather than all chargeable residues, is highly consistent

dx.doi.org/10.1021/jp309135m | J. Phys. Chem. B 2013, 117, 2615−2624

to reported values in the literature[8,16,43] of 5.1, 5.2, and 4.7 for BLGA, BLGB, and BSA, respectively. BLGA has a lower pI than that of BLGB, which is caused by a double-point mutation of D64G/V118A from BLGA to BLGB, where BLGA has one more negative titratable residue than BLGB. Therefore, in the study of protein self-association and its complex with polysaccharides, only residues in the protein surface (i.e., titratable or exposed hydrophobic residues) are considered. Three kinds of patches in the protein surface were then determined according to the location and the charge status of residues. The positive charge patches were composed by positively titratable residues (R, K, H, and N terms), the negative charge patches were made from residues D, E, Y (at high pH only), and C terms, and the hydrophobic patches contained residues A, G, I, L, M, F, P, W, and V. By recording the exact position, the size and the partial charge of each patch using the methods previously described,[35] coarse grained models for these three proteins at different pHs can be constructed, and typical models at pH 5.0 were illustrated in Figure 1. The mutation D64G from BLGA to BLGB slightly

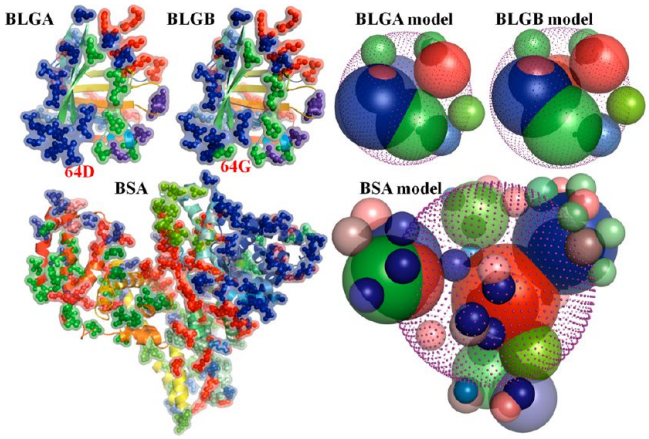

Figure 1. Distribution of charge and hydrophobic patches in BLGA, BLGB, and BSA based on their crystal structures (left) and their corresponding coarse grained models (right) at pH 5.0. Red-color based spheres represent positive charge patches, blue-color based spheres are negative charge patches, and green-color based spheres are exposed hydrophobic patches. The purple meshes in the center of models are the excluded volume of the whole protein. The size of each patch by gyration radius is exactly represented by the radius of each sphere.

decreases the size of the largest negative titratable patch in BLGA and simultaneously increases the size of the largest hydrophobic patch in BLGB. The mutation V118A occurs in the buried region, which does not show any difference in the two coarse grained models for BLGA and BLGB.

Pectin was modeled as a string of soft beads connected at fixed bond length, under the freely jointed chain model for polymers.[44] Each bead with a radius of 0.5 nm corresponds to a disaccharide unit[45,46] and loads a partial charge at the center arising from the dissociation of −COOH group. Conjoined beads have a constant separation of 1.0 nm. The solvent was implicitly modeled as a dielectric continuum. Here, it is worthy to note that, in the simulation model, all charges are located in the center of hard spheres, where Manning condensation[47] can be ignored in electrostatic interaction calculation.

The interaction energy to guide the Monte Carlo simulation was defined as

$$U = \sum_{i,j} [U_{ele}(i, j) + U_{hyd}(i, j) + U_{vdw}(i, j)] \quad (1)$$

The three terms represent electrostatic interaction (ele), hydrophobic potential (hyd), and van der Waals interaction (vdw), respectively. The electrostatic potential was calculated through Debye−Hückcle approximation, which is written as

$$U_{ele}(i, j) = \frac{q_i q_j}{4\pi\varepsilon_0\varepsilon_r r_{ij}} \exp(-r_{ij}/\lambda_D), \quad \forall\ r_{ij} \geq \sigma_{ij} \quad (2)$$

where q_i and q_j are the partial charges brought by the charge patches and polysaccharide (PS) beads, and the constant $(4\pi\varepsilon_0\varepsilon_r)^{-1}$ is set as 2.0 (k_BT*nm/e^2) with e the electric charge unit (e.u.), k_B the Boltzmann constant, and T the absolute temperature. The λ_D is the Debye screening length, which is fixed at 0.974 nm, corresponding to a saline solution with 0.1 M monovalent salt. The r_{ij} is the distance between coarse grained particles i and j, and the cutoff separation distance σ_{ij} is equal to $\sigma_i + \sigma_i$ with σ_i the van der Waals radius of PS beads or charge patches in protein surface.

The hydrophobic interaction has a collective nature, which involves synergetic interactions among macromolecules and solvent molecules. In implicit solvent model, the magnitude of hydrophobic interaction is proportional to the fraction of overlapped surface area (i.e., nonaccessible to solvent area) compared to the whole surface of a spherical particle. Therefore, the hydrophobic interaction can be calculated in a pairwise manner using the definition of

$$U_{hyd}(i, j) = k_{hyd}(i, j)\left\{\frac{1}{4r_{ij}h_i}[h_j^2 - (r_{ij} - h_i)^2]\right\},$$
$$\forall\ \sigma_{ij} < r_{ij} < h_i + h_j \quad (3)$$

where h_i and h_j are the hydration radii of the two particles (see Figure 2). Each equals the van der Waals radius of a particle

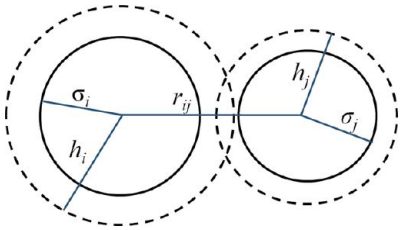

Figure 2. Schematic diagram of hydrophobic interaction. Solid circles are the van der Waals radius, and dashed circles include the hydration layer.

plus 0.14 nm, a probe (e.g., water) size generally used for solvent accessibility evaluation. The prefactors $k_{hyd}(i, j) = [k_{hyd}(i) + k_{hyd}(j)]/2$ and $k_{hyd}(i)$ are $-1.0\ k_BT$ if it is an exposed hydrophobic patch, $0.7\ k_BT$ for the PS bead, and $1.0\ k_BT$ for the charge patch. The $0.7\ k_BT$ of the PS bead was according to the ∼30% methyl esterification of the pectin sample used in previous works.[35,48] The van der Waals interaction was calculated by

$$U_{vdw}(i, j) = U_{rep}(i, j) + U_{att}(i, j) = \varepsilon_{ij}\left(\frac{\sigma_{ij}}{r_{ij}}\right)^{12} - 2\varepsilon_{ij}\left(\frac{\sigma_{ij}}{r_{ij}}\right)^{6} \quad (4)$$

dx.doi.org/10.1021/jp309135m | J. Phys. Chem. B 2013, 117, 2615−2624

where $\varepsilon_{ij} = (\varepsilon_i\ \varepsilon_j)^{0.5}$ with ε_i (fixed at $1.0k_BT$ in this work) the van der Waals potential well and σ_i the van der Waals radii for proteins (PRO), listed in Table 1. The attractive part of van der Waals interaction (U_{att}) was only applied on interactions that involved all the proteins and the PS beads. The steric repulsive part (U_{rep}) was also applied on charge or hydrophobic patches when two particles approached closer than the sum of their van der Waals radii.

Simulation Settings and Complex Identification. Table 2 shows the number of proteins and PS chains used in the simulation of the protein−PS mixture and the control simulation with either the protein or PS alone. In the mixtures, the ratio of the volume fraction of protein to pectin is fixed at 2:1, and each pectin chain contains 200 beads. The total volume fraction of proteins and pectin chains, either in mixture or in control simulations, was also fixed at 2.5%. Monte Carlo simulation was carried out in a cubic box with an edge length of 72 nm and periodic boundary conditions (PBC) applied in all directions. Relaxation of the proteins and polysaccharide chains were carefully tuned and described previously.[34,35] Grossly, PS chains were relaxed through crankshaft rotation, pivot rotation, and snake-slithering movement, while proteins as a rigid body can be relaxed by either random translation or spinning around a random axis passing its center. Attempting configuration was updated according to Metropolis rule.[49] To achieve configurations under thermodynamic equilibrium, proteins and PS chains were first evenly dispersed in a simulation box, followed by 6×10^5 MCS relaxation guided by U_{rep}. Here, each MCS represents the simulation time where all PS beads and all patches in proteins have one attempted movement on average. Then another 6×10^5 MCS simulation with all energy terms was carried out based on the final configuration after the relaxation guided by U_{rep}. Snapshots of simulation configurations were recorded in every 5×10^3 MCS in each trajectory. Finally, for simulation results analysis, we collected 100 configurations by taking the final 25 configurations from four parallel trajectories. The four parallel trajectories were generated from different initial configurations and different random seeds.

Table 2. Number of Proteins (PRO) and Pectin Chains in Simulation Systems with the Whole Volume Fraction Fixed at 2.5%, and the Volume Ratio of Protein to Polysaccharide Is 2:1 in the Mixtures

system	BLGA or BLGB	BSA	pectin
mixtures	448	56	30
control	664	83	90

A complex was identified if any one protein and one pectin chain had an intermolecular interaction stronger than Γk_BT with Γ being a negative constant. The intermolecular interaction was calculated by eq 1, through the summation of all interaction pairs between these two molecules. Besides the strong association of proteins and PS chains, the complex can be further enlarged through the self-association of proteins and the entanglement of PS chains. We labeled the complex accumulatively enlarged through these three pathways as type I, II, and III complex, respectively. Type I and type II complexes were dominated by a competition between short-range

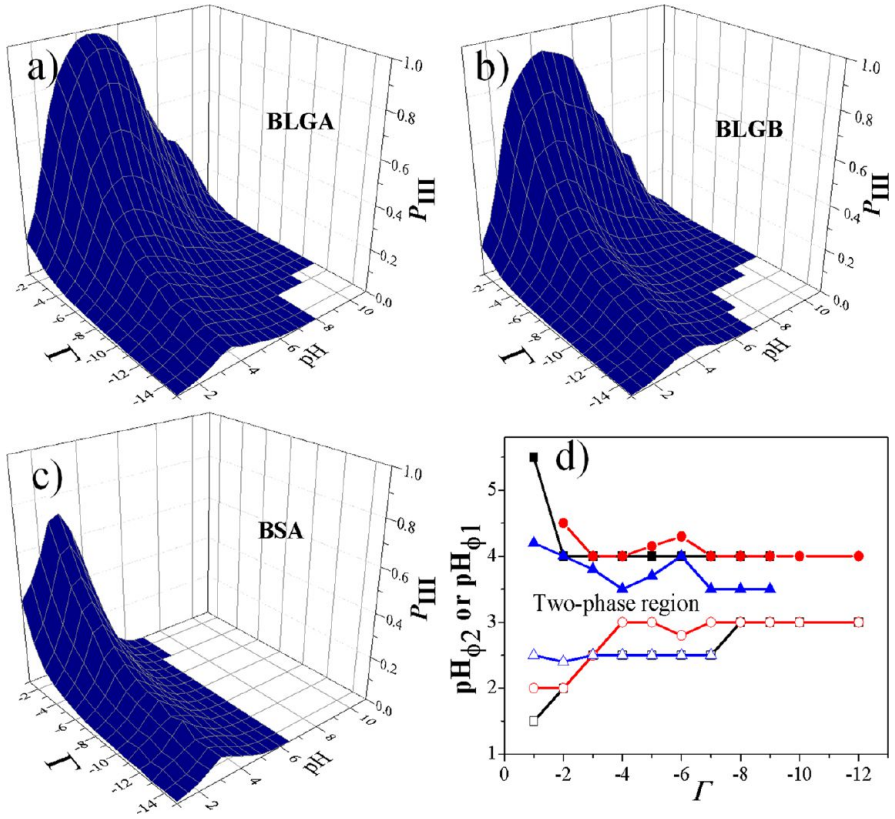

Figure 3. Percolation probability (P_{III}) plotted against pH and different Γ cutoffs based on simulations in mixtures of pectin and (a) BLGA, (b) BLGB, and (c) BSA. The complex coacervate phase boundaries were also plotted against Γ as shown in panel d. In panel d, solid points are $pH_{\Phi1}$ and empty points represent $pH_{\Phi2}$, square, circle, and triangle indicate the data from the pectin mixtures with BLGA, BLGB, and BSA, respectively.

dx.doi.org/10.1021/jp309135m | J. Phys. Chem. B 2013, 117, 2615−2624

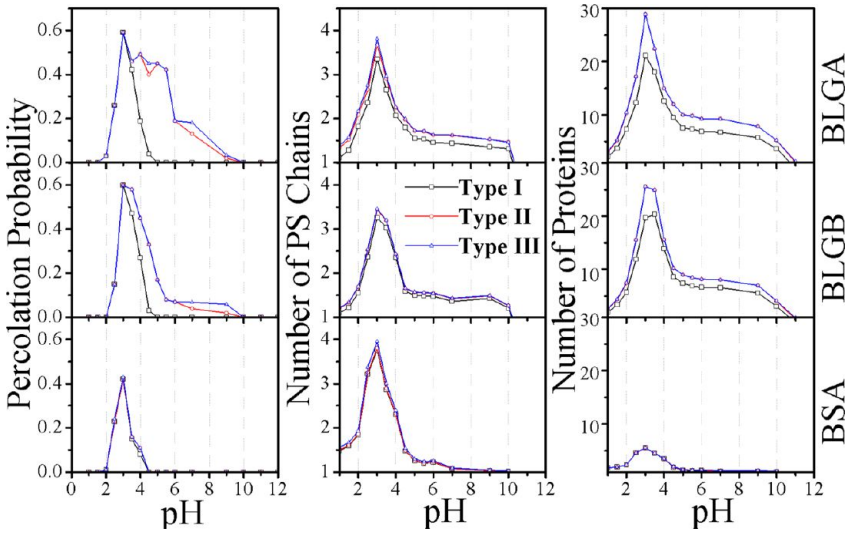

Figure 4. Percolation probability of simulation configuration(left), the average number of PS chains (middle) and the average number of proteins (right) in type I, II, and III complexes and complex coacervate at $\Gamma = -5$ from mixtures of pectin with BLGA, BLGB, and BSA.

attractions including hydrophobic interaction, van der Waals and electrostatic attraction, and long-range repulsions majorly contributed from electrostatic interaction among likely charged patches and beads. The type III complex was not decided by the magnitude of intermolecular interactions on the basis of the type II complex, but a topological constraint transitorily created by PS chains. Type I complex is the core of the complex, which counts the strong association between protein and PS chains, type II complex also considers the expansion via the self-association of proteins, and type III complex further accounts the enlargement of the complex through the entanglements of PS chains. A complex grows and eventually can form a complex coacervate once it forms a percolated complex domain in the simulation box with periodic boundary conditions. Such a percolated complex domain maintained through strong intermolecular association allows it to sustain the structure under some mechanical stress rather than flow to dissipate energy, which matches the feature of coacervate phase. Further, since the percolation concepts have been successfully engaged to describe physical gelation[50−52] and coacervate phase domains or complex particles usually share high similarity with gel in internal structures and interactions,[53−55] it is reasonable to regard percolated complex domain as complex coacervate. Accordingly, the percolation probability, which was defined as the fraction of simulation configurations with percolated complex in all the 100 configurations, can be used to determine the phase boundary of complex coacervation.

RESULTS AND DISCUSSION

Complex Coacervation Phase Boundary. First, the percolation probability of type III complex (P_{III}) was used to evaluate the probability of a sample in which liquid−liquid phase separation occurs at a given pH and the cutoff of intermolecular interaction (Γ). The profiles of P_{III} from BLGA, BLGB, BSA, and pectin mixtures and the phase boundaries indicated by $pH_{\Phi 1}$ and $pH_{\Phi 2}$ are shown in Figure 3. The $pH_{\Phi 1}$ and $pH_{\Phi 2}$ correspond to the onset and the disassociation of complex coacervate (i.e., the steep increase/decrease of P_{III}) with the decrease of pH. They can be used to compare with the critical pH values associated with complex coacervate determined from turbidimetric titration experiments, which have been widely used in the literature.[56] It can be seen that BLGA and BLGB have higher probabilities and broader pH windows to form complex coacervate than BSA. BLGA also has a higher percolation probability than that of BLGB, though it only contains one more negative titratable residue. This suggests that the strong self-association proneness of BLGA can overcome the potentially stronger electrostatic repulsion with pectin than that of BLGB to strengthen complex coacervation. The percolation probability expanded to quite a high pH at small intermolecular interactions cutoff. It suggests that the binding of protein and pectin can occur at pH far above pI. This agrees with previous reports of binding occurring "on the wrong side of pI"[7,57,58] and verified the importance of the charge patch concepts toward the understanding of protein and polysaccharide complex coacervation. The complex coacervate could diminish if the intermolecular interaction was required up to $-12k_BT$, which was close to around $-16k_BT$ (i.e., −10 kcal/mol) binding affinity between BLG and pectin measured by ITC by Girard et al.[59] The pH window for the complex coacervate was also consistent with previous experimental observations in 0.1 M saline solutions.[48,60,61] The two-phase region of complex coacervate was suppressed in smaller pH window when stronger intermolecular association was engaged. This phase diagram is very similar to the salt-screening effect in protein−polysaccharide complex observed from turbidimetric titration.[48,62] It suggests the electrostatic interaction may still dominate the complex coacervation in these pectin and protein systems.

Further, in order to make clear how self-association of proteins contributed to complex coacervation, the percolation probability, the average size of complex counted by the number of either PS chains or proteins at a given intermolecular interaction cutoff ($\Gamma = -5$) against pH was plotted and shown in Figure 4. The pH window for type I complex coacervation in the three systems is from pH 2.0 to 5.0. The pH window for the complexation is consistent with experimental observations of BLG and pectin[48] and BSA and pectin mixtures.[35] With the help of protein self-association, for type II complex, the pH window can expand to pH 10.0 in pectin mixtures with BLGA and BLGB. Entanglement of PS chains, as shown by the size of the complex counted by the number of pectin chains, has minor

dx.doi.org/10.1021/jp309135m | J. Phys. Chem. B 2013, 117, 2615−2624

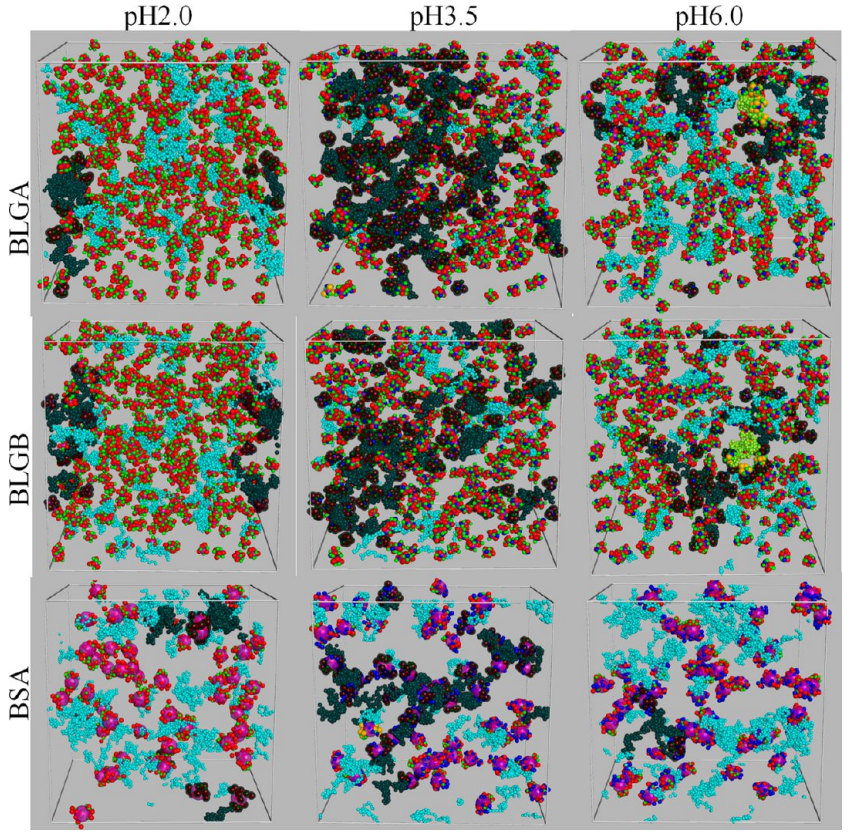

Figure 5. Snapshots of simulation configurations under thermodynamic equilibrium; complex was identified by intermolecular interaction stronger than $-5k_BT$. Red, blue, and green spheres are positive charge, negative charge, and exposed hydrophobic patches in protein surface; purple bubbles represent the excluded volume of the whole protein, and pectin beads are cyan. The black colored out the largest type I aggregate in each configuration, and the yellow colored out the aggregate attaching to the largest type I aggregate through protein self-association (type II aggregate).

influence to complex coacervation at all pHs. In the three systems, it was found that the maximum of the percolation probability and the average size of complex were overlapped at pH 3.0, but the average number of proteins in complex is much larger in BLGA and BLGB than that of BSA−pectin mixtures. This also correlated to the higher percolation probability in the former two systems. Therefore, higher self-association proneness of BLGA and BLGB not only increases the percolation probability and the complex size but also expands the pH windows for complex coacervation.

Simulation Snapshots. Figure 5 presents typical snapshots of simulation configurations under thermodynamic equilibrium. The complex was identified using the intermolecular interaction cutoff of $-5k_BT$. The pH values selected were at the lower pH boundary (pH 2.0) where proteins interact with almost neutral PS chains, at intermediate pH where complex coacervate largely formed (pH 3.5) and the upper pH limit where protein−pectin complex was suppressed (pH 6.0) due to they are likely charged. At low pH, van der Waals attraction (U_{att}) and hydrophobic interaction were in charge of the complexation, molecules should approach close enough to get sufficient attractive strength. Therefore, it can be seen that the complex at low pH was made of closely packed molecules. At intermediate pH (lower than the pI of proteins), proteins and pectin chains brought opposite charges, and they have strong binding affinity through electrostatic attraction. Electrostatic interaction dominates hydrophobic and van der Waals interactions in complexation. The long-range nature of electrostatic interaction allows the complex to have broadly spatial expansion and more molecules entrapped in the domain, which leads to high percolation probability. When pH is higher than the pI of proteins, proteins brought likely charges as that of pectin chains. Protein−polysaccharide binding was limited to the oppositely charged patches, and the extent of protein self-association was strongly dominated by the specific distribution of patches in protein surface. Complex associations between proteins and polysaccharides were suppressed due to electrostatic repulsion from neighboring patches with likely charges. However, protein self-association may have less impact due to the match of patches with complementary location, charge, and hydrophobicity. Thus, the contribution from protein self-association became important to complex coacervation. Since BLGA and BLGB bring less negative charges than BSA and protein self-association of BSA is very weak, at high pH, the BSA−pectin complex is too weak to form complex coacervate. Contrarily, complex coacervate in BLG−pectin mixtures still can be observed, which is majorly contributed from the self-association of proteins.

Association of Molecules. The distribution and the association of molecules in simulation configurations can be viewed through the pair correlation function (PCF) and the second virial coefficient (B). They were calculated using the following definitions

$$\mathrm{PC}F_{XY}(r) = \frac{\sum_i \sum_j \delta(r - r_{ij})}{4\pi r^2 C_{XY}} \quad (5)$$

dx.doi.org/10.1021/jp309135m | J. Phys. Chem. B 2013, 117, 2615−2624

$$B_{XY} = \frac{1}{N_{XY}} \sum_i \sum_j r_{ij}^2 \{1 - \exp[-U(i,j)/k_B T]\} \quad (6)$$

where X and Y are PS beads or proteins (PRO), C_{XY} is a constant used to normalize long-range correlation to unit value. $\delta(t)$ is the delta function that equals 1 if t equals 0; all else is zero. N_{XY} is the total number of interaction pairs between X and Y. The r_{ij} and $U(i,j)$ are the distance and the interaction energy between two particles i and j. The PCF values is larger than 1 and indicates the enrichment of the two kinds of molecules at given separation distance, else less than 1 suggests the depletion of the two molecules at given correlation length. A negative B value indicates two kinds of particles are attractive, and a positive one corresponds to repulsive interaction. The magnitude of B values is proportional to the binding affinity or the repelling strength of two kinds of particles in the simulation system.

The PCF profiles against separation distance at different pHs calculated from protein and pectin mixtures and their control simulation systems are presented in Figure 6 and Figure S2 (in Supporting Information). According to the PS-PRO PCF profiles, both BLGA and BLGB have strong associations from around 2.5 to 6.5 nm and BSA from 4.1 to 9.5 nm in the pH window where complexes with pectin largely occurs. BSA has a narrower pH window with upper pH 5.0 verses pH 7.0 in BLGA, BLGB and pectin mixtures, which is consistent with the phase boundaries determined by percolation probability with an intermolecular interaction cutoff of $-5k_BT$. The PRO-PRO PCF profiles indicate that BLGA and BLGB have similar enrichment around 4.5 nm, and BSA shows bimodal enrichment at 6.5 and 9.1 nm in the mixtures at pH range from 4.0 to 9.0. The PRO-PRO PCF profiles from control simulations are very similar to those from the mixtures, except the enrichments of proteins become less prominent as indicated by the lower height of peaks. Additionally, the bimodal peaks for the enrichment of BSA in control simulation shift to larger separation distance of 8.2 and 10.4 nm, respectively. This result suggests that the presence of PS chains can not only promote local enrichment of proteins but also lead to closer packing of proteins. The bimodal distribution of BSA is from the specific distribution of patches in the surface of BSA, which introduces anisotropic interaction and steric repulsion around BSA molecules. In the consideration of interchain PCF profiles of PS beads, the local enrichment of PS beads is significant in protein−pectin mixtures comparing with the one from pure pectin systems. BLGA and BLGB have stronger promotion of the enrichment of PS beads than BSA in the complex pH window. It can be understood that less amount of binding of larger proteins (BSA) have less influence on the arrangement of PS chains, while binding of many small proteins can significantly reduce electrostatic repulsion among PS chains. Overall, the PCF profiles indicate that there is a stronger affinity of BLGA and BLGB than BSA to form complex with pectin. The former two have stronger enrichment of PS chains in the pH window for complexes, which in-turn facilitate complex coacervation. Accounting the minor differences in BLGA and BLGB, it did not bring significant influences on all the distribution of molecules.

Three types of the second virial coefficients as a function of pH were shown in Figure 7. All three proteins show the strongest binding affinity with pectin at the vicinity of pH 3.0, which matches the highest percolation probability of type I complex as shown in Figure 4. BSA−pectin is weakly attractive when pH is higher than 5.0, while BLGA and BLGB are still attractive to pectin chains up to pH 10.0. Interactions among pectin chains in mixtures are always repulsive, and the repelling strength increases with pH. Weak attraction among PS chains in pectin control systems at low pH, where almost neutral PS chains can aggregate together contributed from van der Waals interaction. The repelling strength of pectin chains in BSA and control are very similar, which is remarkably larger than that in BLGA or BLGB mixtures. This is consistent with BSA having a weaker promotion for local enrichment of PS chains and binding of a large amount of BLGA and BLGB can efficiently reduce interchain repulsion as discussed previously. The secondary virial coefficients of protein−protein interaction are

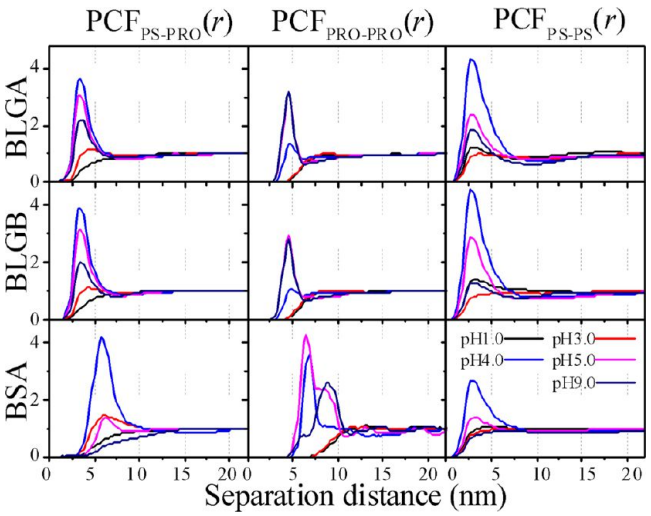

Figure 6. Pair correlation function profiles from BLGA, BLGB, and BSA and pectin complex systems presented by three kinds of correlations at different pHs.

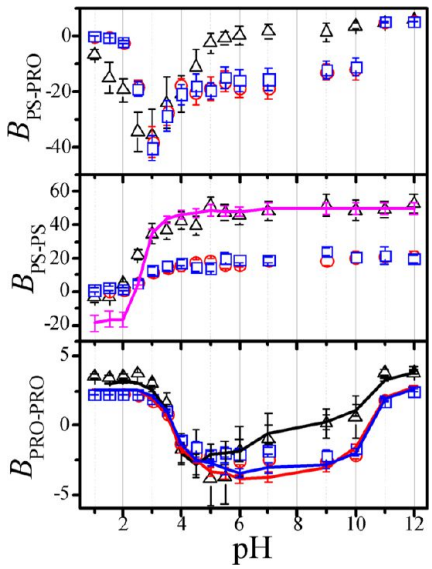

Figure 7. Second virial coefficient for three kinds of molecular association. The square, circle, and triangle are from the pectin mixtures with BLGA, BLGB, and BSA, respectively, and the lines are from the corresponding control simulation systems with BLGA (red), BLGB (blue), BSA (black), and pectin (purple) alone.

dx.doi.org/10.1021/jp309135m | J. Phys. Chem. B 2013, 117, 2615−2624

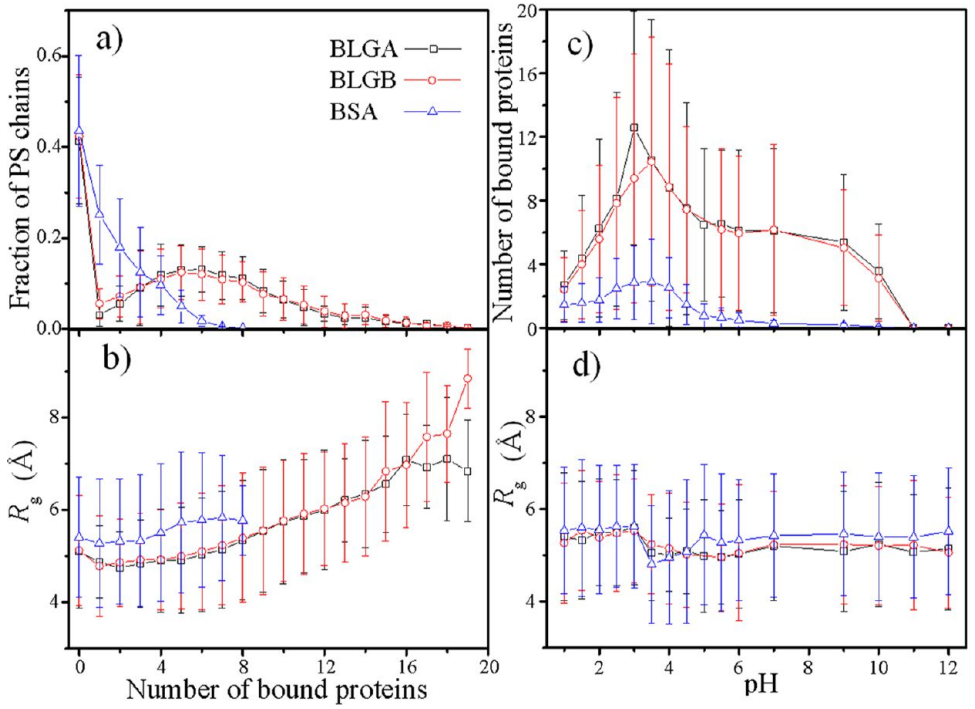

Figure 8. (a,b) Distribution and the average size of PS chains against the number of bound proteins; (c,d) the number of bound proteins per PS chain and the conformation of PS chains as a function of pH presented at $\Gamma = -5$.

relatively weak, and the pH dependence has minor difference between the one from protein−pectin mixtures and that from control systems. BSA proteins were slightly attractive in a narrow pH window from 4.0 to 7.0; BLGA and BLGB were attractive in a broad pH window from 4.0 to 10.0. At pH 5 and 5.5, the attraction in mixtures was stronger than that from the control with BSA alone. This could be contributed by the depletion potential arising from the presence of pectin chains, an enrichment of proteins through entropic optimization. From pH 6.0 to 10.0, the protein−protein attraction in BLGA is stronger than that in BLGB−pectin mixtures. Coupling with the higher percolation probability at this pH range as shown in Figure 3, it reveals that the stronger complex capability with pectin at pH above the pI of protein in BLGA is directly contributed from the stronger self-association proneness of BLGA. Though the second virial coefficients provided a consistent trend associated with complex coacervation, they are tightly coupled with the contribution from three different interactions. The maximum of the hydrophobic interaction and the van der Waals interaction are approximately at the same level in current simulation settings, but the former may be stronger according to their roles in protein folding.[63] It is worthy but difficult to address the exact prefactor values for these different interactions, especially in coarse grained models, and our in-depth study is still ongoing.

Conformation of Pectin Chains. In Figure 8, the distribution and the gyration radius of pectin chains as a function of the number of bound proteins (intermolecular interaction cutoff of $-5k_BT$) and pH was presented. In all the plots, the big error bars are caused by strong intermolecular associations. The associations create heterogeneous domains in the system and cause diverse distributions of the conformation of pectin chains and the bound molecular pairs. The fraction of PS chains monotonously decrease with an increased number of bound proteins in BSA−pectin mixtures, while an enrichment of PS chains with 4 to 7 bound proteins was observed in BLGA and BLGB and pectin mixtures. The enrichment may be contributed from two aspects. One is the size of BLG, which is one-eighth of that of BSA; binding of BLG introduces less steric hindrance to allow PS chains to bind more. The second contribution may be that the strong self-association of BLG, which makes proteins cluster. Pectin chains binding to one protein also tend to bind others in the same cluster.

The size of PS chains increase with the number of bound proteins, which is consistent with previous findings in protein-rich mixtures.[35] At the same number of bound proteins, pectin chains have a larger size in BSA mixtures than those in BLG mixtures. This is reasonable because BSA is larger than BLG, and pectin chains need to be more extended to minimize the steric repulsion aroused by BSA. In BLG−pectin mixtures, when PS chains bind more than 16 proteins (note, such PS chains only occur in pH from 2.5 to 4.0), the size of PS chains in BLGB mixtures is larger than that in BLGA mixtures. This may be related to that BLGB had less electrostatic repulsion and larger hydrophobic attraction with pectin chains than BLGA and that BLGB has less self-association to form less protein clusters, which requires pectin chains to be more extended to bind more BLGB proteins. Therefore, the dependence of the number of bound proteins of the gyration radius of pectin chains in BLGA and BLGB and pectin mixtures revealed that although BLGB has a stronger attraction to pectin chains than BLGA, the stronger self-association proneness of BLGA assists it to have similar complex coacervation behavior as that in BLGB−pectin mixtures.

In the pH window for complex coacervation, the average number of bound proteins per PS chain has large values. Pectin chains have less bound BSA than BLGA and BLGB, which is due to the differences in both size and binding affinity. Similar to previous simulations,[34,35] the gyration radius of PS chains had no obvious dependence on pH. The failure to see the

dx.doi.org/10.1021/jp309135m | J. Phys. Chem. B 2013, 117, 2615−2624

electric persistence length[64] on the conformation of pectin chains is understandable. To see the influence of electrostatic interaction on the total persistence length and the conformation of pectin chains, the interaction range of electrostatic repulsion must be larger than the diameter of the pectin bead ($2\sigma_{PS}$), and the electrostatic repulsion must be larger than the van der Waals attraction at $2\sigma_{PS}$. In current simulation works, the former condition was satisfied, but the latter one was not achieved. Future simulations in consideration of such restrictions to observe charge induced rigidity of polysaccharide chains and its influence to the complex coacervation with protein is ongoing.

Binding Sites in Proteins. When protein−pectin complexes form through nonselective electrostatic interaction and hydrophobic interaction, the strongest binding sites in proteins are highly overlapped with charge patches and hydrophobic patches. The patches that have on average the strongest attraction at different pHs were identified and listed in Table S1 (in Supporting Information). In BLG A and B, residue 111A forms a small hydrophobic patch, which was the furthest from the center of the protein. This patch becomes the strongest binding site in either protein−pectin mixtures or the protein systems through hydrophobic interaction when pH is far from the pI of protein. Patch III in BLGB involving the mutation site D64G from BLGA, also acts as the strongest binding site at pH 1.0 in the BLGB−pectin mixture through hydrophobic interaction. In the pH window for complexes, the second largest and most protruding positive patch made of 75K, 77K, 83K, 91K, and N terms always dominates the strongest binding site in BLGA and BLGB and pectin mixtures. In the corresponding control simulation of BLGA or BLGB systems, the strongest binding sites may vary in several positive or negative patches. The mutation site D64G showed up as the strongest binding site from pH 4.0 to 5.0 in BLGA control systems. This agrees with recent reports in the study of BLGA and BLGB binding to cationic particles that a large negative charge patch in BLGA promoted the binding.[7,16] In the control systems, when pH is above the pI of protein, the strongest binding sites are more convergent at a large positive charge patch in BLGA than that in BLGB. This indicates that the minor difference between BLGA and BLGB with a double mutation of D64G/V118A is responsible to promote protein self-association through interaction with the second largest and most protruding positive patch in BLGA.

Hydrophobic binding sites were also shown to be the strongest binding sites when pH is out of the pH window for complex in BSA−pectin mixtures. At pH from 6.0 to 11.0, the most protruding positive patch made of 564K, 557K, 560K, 574K, 573K, and 510H dominates the strongest binding site, which is the same as that observed previously.[35] This suggests that the introduction of hydrophobic patches in proteins will not significantly change the strongest binding of BSA with pectin in the pH window for complexes. While accounting for the binding sites from BSA control systems, hydrophobic patches were largely overlapped with the strongest binding sites. In comparison of the patches in BLGA and BLGB control systems, self-association of BSA was majorly dominated by hydrophobic interactions, which are weaker than electrostatic interactions. Therefore, the stronger self-association proneness in BLG than BSA may be that either charge patches or hydrophobic patches are the most important binding sites.

CONCLUSIONS

Coarse grained Monte Carlo simulation was utilized to study the influence of self-association proneness of three proteins in complex coacervation with pectin. It was found that the difference between the two isomers of beta-lactoglobulin (A and B) did not bring any significant influence on the complex coacervation except in the self-association of proteins. The remarkable difference in size and surface between BLG and BSA leads to distinct complex profiles with pectin. An increase of self-association proneness from BSA to BLG was contributed by dominating force changes from weak hydrophobic interactions to electrostatic interactions. The increase of self-association from BLGB to BLGA was a result of large negatively charged patches in BLGA, which promoted electrostatic interactions of the second largest and most protruding positive charge patch. The stronger self-association proneness of BLG not only strengthened complex coacervate but also expanded the pH window for complex coacervation. A simple method was introduced to calculate hydrophobic interactions, and it was found that the hydrophobic patches in the proteins coarse grained model had key importance to understanding the influence of self-association proneness in protein complexes.

ASSOCIATED CONTENT

Supporting Information

Table S1 presents the whole lists of residues in the strongest binding sites at different pHs for BLGA, BLGB, and BSA; Figure S1 shows the partial charges in the whole protein or in the protein surface as a function of pH; Figure S2 demonstrates the pairwise correlation functions from protein control simulation systems. This material is available free of charge via the Internet at http://pubs.acs.org.

AUTHOR INFORMATION

Corresponding Author

*Tel: 848-932-5514. Fax: 732-932-6776. E-mail: qhuang@aesop.rutgers.edu.

Notes

The authors declare no competing financial interest.

ACKNOWLEDGMENTS

This work was supported by Department of Agriculture National Research Initiative (#2009-35603-05071). We thank Dr. David A. Joiner at Kean University for supporting the computational resource for this work, funded by National Science Foundation project OCI-0722790.

REFERENCES

(1) Jones, O. G.; McClements, D. J. *Adv. Colloid Interface Sci.* **2011**, *167*, 49−62.
(2) Xing, F.; Cheng, G.; Yi, K.; Ma, L. *J. Appl. Polym. Sci.* **2005**, *96*, 2225−2229.
(3) Weinbreck, F.; Minor, M.; De Kruif, C. G. *J. Microencapsulation* **2004**, *21*, 667−679.
(4) Huang, M.; Vitharana, S. N.; Peek, L. J.; Coop, T.; Berkland, C. *Biomacromolecules* **2007**, *8*, 1607−1614.
(5) George, M.; Abraham, T. E. *J. Controlled Release* **2006**, *114*, 1−14.
(6) Chaniotakis, N. A. *Anal. Bioanal. Chem.* **2004**, *378*, 89−95.
(7) Xu, Y.; Mazzawi, M.; Chen, K.; Sun, L.; Dubin, P. L. *Biomacromolecules* **2011**, *12*, 1512−1522.
(8) Klostergaard, H.; Pasternak, R. A. *J. Am. Chem. Soc.* **1957**, *79*, 5671−5674.
(9) Ogston, A. G.; Tombs, M. P. *Biochem. J.* **1957**, *66*, 399−403.

(10) Timasheff, S. N.; Townend, R. *J. Am. Chem. Soc.* **1958**, *80*, 4433−4434.
(11) Piazza, R.; Iacopini, S.; Galliano, M. *Europhys. Lett.* **2002**, *59*, 149−154.
(12) Majhi, P. R.; Ganta, R. R.; Vanam, R. P.; Seyrek, E.; Giger, K.; Dubin, P. L. *Langmuir* **2006**, *22*, 9150−9159.
(13) Levi, V.; González Flecha, F. L. *Biochim. Biophys. Acta* **2002**, *1599*, 141−148.
(14) Mansouri, A.; Haertlé, T.; Gérard, A.; Gérard, H.; Guéant, J. L. *Biochim. Biophys. Acta* **1997**, *1357*, 107−114.
(15) Noel, T. R.; Krzeminski, A.; Moffat, J.; Parker, R.; Wellner, N.; Ring, S. G. *Carbohydr. Polym.* **2007**, *70*, 393−405.
(16) Chen, K. M.; Xu, Y. S.; Rana, S.; Miranda, O. R.; Dubin, P. L.; Rotello, V. M.; Sun, L. H.; Guo, X. H. *Biomacromolecules* **2011**, *12*, 2552−2561.
(17) Kosters, H. A.; Wierenga, P. A.; de Vries, R.; Gruppen, H. *Biomacromolecules* **2011**, *12*, 2159−2170.
(18) Kosters, H. A.; Wierenga, P. A.; Gruppen, H. *Food Hydrocolloids* **2010**, *24*, 667−673.
(19) Sperber, B. L. H. M.; Cohen Stuart, M. A.; Schols, H. A.; Voragen, A. G. J.; Norde, W. *Biomacromolecules* **2009**, *10*, 3246−3252.
(20) Sperber, B. L. H. M.; Cohen Stuart, M. A.; Schols, H. A.; Voragen, A. G. J.; Norde, W. *Biomacromolecules* **2010**, *11*, 3578−3583.
(21) Tozzini, V. *Curr. Opin. Struct. Biol.* **2005**, *15*, 144−150.
(22) van der Kamp, M. W.; Shaw, K. E.; Woods, C. J.; Mulholland, A. J. *J. R. Soc. Interface* **2008**, *5*, 173−190.
(23) Vitalis, A.; Pappu, R. V. Methods for Monte Carlo Simulations of Biomacromolecules. In *Annual Reports in Computational Chemistry*; Ralph, A. W., Ed.; Elsevier: New York, 2009; Vol. *5*, pp 49−76.
(24) Richards, F. M. *Annu. Rev. Biophys. Bioeng.* **1977**, *6*, 151−176.
(25) Skepo, M.; Linse, P. *Macromolecules* **2003**, *36*, 508−519.
(26) Carlsson, F.; Malmsten, M.; Linse, P. *J. Am. Chem. Soc.* **2003**, *125*, 3140−3149.
(27) Akinchina, A.; Linse, P. *Macromolecules* **2002**, *35*, 5183−5193.
(28) Bianchi, E.; Blaak, R.; Likos, C. N. *Phys. Chem. Chem. Phys.* **2011**, *13*, 6397−6410.
(29) da Silva, F. L. B.; Jönsson, B. *Soft Matter* **2009**, *5*, 2862−2868.
(30) Cooper, C. L.; Goulding, A.; Kayitmazer, A. B.; Ulrich, S.; Stoll, S.; Turksen, S.; Yusa, S.-I.; Kumar, A.; Dubin, P. L. *Biomacromolecules* **2006**, *7*, 1025−1035.
(31) de Vries, R. *J. Chem. Phys.* **2004**, *120*, 3475−3481.
(32) Carlsson, F.; Malmsten, M.; Linse, P. *J. Phys. Chem. B* **2001**, *105*, 12189−12195.
(33) Carlsson, F.; Linse, P.; Malmsten, M. *J. Phys. Chem. B* **2001**, *105*, 9040−9049.
(34) Li, Y.; Shi, T.; Huang, Q.; An, L. *J. Phys. Chem. B* **2012**, *116*, 3045−3053.
(35) Li, Y.; Zhao, Q.; Huang, Q. *Carbohydr. Polym.* **2012**, submitted.
(36) Shazman, S.; Celniker, G.; Haber, O.; Glaser, F.; Mandel-Gutfreund, Y. *Nucleic Acids Res.* **2007**, *35*, W526−W530.
(37) Barzegar, A.; Moosavi-Movahedi, A. A.; Mahnam, K.; Ashtiani, S. H. *Carbohydr. Res.* **2010**, *345*, 243−249.
(38) Huang, B.; Liu, F. F.; Dong, X. Y.; Sun, Y. *J. Phys. Chem. B* **2011**, *115*, 4168−4176.
(39) Li, Y.; Zhang, Y. *Proteins: Struct., Funct., Bioinf.* **2009**, *76*, 665−676.
(40) Kabsch, W.; Sander, C. *Biopolymers* **1983**, *22*, 2577−2637.
(41) Tanford, C.; Kirkwood, J. G. *J. Am. Chem. Soc.* **1957**, *79*, 5333−5339.
(42) Pace, C. N.; Grimsley, G. R.; Scholtz, J. M. *J. Biol. Chem.* **2009**, *284*, 13285−13289.
(43) Li, Y.; Lee, J.; Lal, J.; An, L.; Huang, Q. *J. Phys. Chem. B* **2008**, *112*, 3797−3806.
(44) Flory, P. J. *J. Chem. Phys.* **1949**, *17*, 303−310.
(45) Marszalek, P. E.; Li, H.; Oberhauser, A. F.; Fernandez, J. M. *Proc. Natl. Acad. Sci. U.S.A.* **2002**, *99*, 4278−4283.
(46) Marcelo, G.; Saiz, E.; Tarazona, M. P. *Biophys. Chem.* **2005**, *113*, 201−208.
(47) Manning, G. S. *J. Chem. Phys.* **1969**, *51*, 924−933.
(48) Wang, X.; Wang, Y.-W.; Ruengruglikit, C.; Huang, Q. *J. Agric. Food Chem.* **2007**, *55*, 10432−10436.
(49) Metropolis, N.; Rosenbluth, A. W.; Rosenbluth, M. N.; Teller, A. H.; Teller, E. *J. Chem. Phys.* **1953**, *21*, 1087−1092.
(50) Li, Y.; Shi, T.; An, L.; Lee, J.; Wang, X.; Huang, Q. *J. Phys. Chem. B* **2007**, *111*, 12081−12087.
(51) Li, Y.; Shi, T.; Sun, Z.; An, L.; Huang, Q. *J. Phys. Chem. B* **2006**, *110*, 26424−26429.
(52) Li, Y.; Sun, Z.; Shi, T.; An, L. *J. Chem. Phys.* **2004**, *121*, 1133−1140.
(53) Schmitt, C.; Sanchez, C.; Desobry-Banon, S.; Hardy, J. *Crit. Rev. Food Sci. Nutr.* **1998**, *38*, 689−753.
(54) Dickinson, E. *Soft Matter* **2008**, *4*, 932−942.
(55) Picone, C. S. F.; da Cunha, R. L. *Food Hydrocolloids* **2010**, *24*, 502−511.
(56) Kaibara, K.; Okazaki, T.; Bohidar, H. B.; Dubin, P. L. *Biomacromolecules* **2000**, *1*, 100−107.
(57) de Vries, R.; Weinbreck, F.; de Kruif, C. G. *J. Chem. Phys.* **2003**, *118*, 4649−4659.
(58) Biesheuvel, P. M.; Stuart, M. A. C. *Langmuir* **2004**, *20*, 2785−2791.
(59) Girard, M.; Turgeon, S. L.; Gauthier, S. F. *J. Agric. Food Chem.* **2003**, *51*, 4450−4455.
(60) Bedie, G. K.; Turgeon, S. L.; Makhlouf, J. *Food Hydrocolloids* **2008**, *22*, 836−844.
(61) Ru, Q.; Wang, Y.; Lee, J.; Ding, Y.; Huang, Q. *Carbohydr. Polym.* **2012**, *88*, 838−846.
(62) Weinbreck, F.; de Vries, R.; Schrooyen, P.; de Kruif, C. G. *Biomacromolecules* **2003**, *4*, 293−303.
(63) Schulz, G. E.; Schirmer, R. H. *Principles of Protein Structure*; Springer: New York, 1977.
(64) Dobrynin, A. V. *Macromolecules* **2005**, *38*, 9304−9314.